State-dependent seismic fragility functions for Italian reinforced concrete structures: preliminary results

Mabel Orlacchio

Dipartimento di Strutture per l'Ingegneria e l'Architettura, Università degli Studi di Napoli Federico II, via Claudio 21,80125 Napoli, Italy. E-mail: mabel.orlacchio@unina.it.

Eugenio Chioccarelli

Dipartimento di Ingegneria Civile, dell'Energia, dell'Ambiente e dei Materiali, Università degli Studi Mediterranea di Reggio Calabria, via dell'Università, 25, 89124, Reggio Calabria, Italy. E-mail: eugenio.chioccarelli@unirc.it.

Georgios Baltzopoulos

Dipartimento di Strutture per l'Ingegneria e l'Architettura, Università degli Studi di Napoli Federico II, via Claudio 21,80125 Napoli, Italy. E-mail: georgios.baltzopoulos@unina.it.

Iunio Iervolino

Dipartimento di Strutture per l'Ingegneria e l'Architettura, Università degli Studi di Napoli Federico II, via Claudio 21,80125 Napoli, Italy. E-mail: iunio.iervolino@unina.it.

The present paper deals with the analytical assessment of structural vulnerability models for Italian reinforced concrete buildings that constitutes one of the results of the ongoing research project RISE (*Real-time earthquake rIsk reduction for a ReSilient Europe*). The structures under consideration are taken from the outcomes of the SERA project (*Seismology and Earthquake Engineering Research Infrastructure Alliance for Europe*) and refer to existing reinforced concrete residential Italian buildings.
State-dependent fragility curves are evaluated via back-to-back incremental dynamic analyses using equivalent-single-degree-of-freedom systems. The analyses consider four damage states, identified by transient maximum inelastic displacement thresholds defined on the system's backbone curve, and are performed with the DYANAS software. Such fragilities are required to calculate the seismic structural reliability when it is possible for structural failure to be reached progressively, i.e., due to the cumulative effect of multiple earthquakes.

Keywords: sequence-based seismic reliability, back-to-back IDA, damage accumulation, SDOF systems, reinforced concrete.

1. Introduction

One of the challenges facing the ongoing research project RISE (*Real-time earthquake rIsk reduction for a ReSilient Europe*) is accounting for earthquake sequences in short-term seismic risk assessment. This requires allowing for the fact that structural failure can occur not only due to a single seismic event, but can also be reached progressively, due to damage accumulation in multiple earthquakes.

Seismic fragility functions are surrogate structural models that provide a structure's conditional probability of failure, given a certain level of seismic intensity in a single event. In this context, failure refers to a structure failing to meet some performance objective. An extension is represented by *state-dependent* fragility functions, that provide the probability that an already-damaged structure makes a transition from a damage state to another (worse) one, given the value of ground motion intensity. The evaluation of state-dependent fragility is a necessary ingredient to account for damage accumulation in multiple events in risk assessment (e.g., Iervolino et al. 2016, Iervolino et al. 2020).

Evaluation of structure-specific fragility functions can be made via non-linear dynamic analysis of a numerical model of the structure. Past research has suggested that the assessment of fragility functions representing structural typologies (or classes) can also be performed applying the same method to a limited number of structures, deemed representative of the entire class (e.g., Iervolino et al. 2007; Kazantzi and Vamvatsikos 2015).

This paper presents a preliminary computation of the state-dependent fragility functions for the Italian reinforced concrete (RC) residential structure classes as identified in the SERA (*Seismology and Earthquake Engineering Research Infrastructure Alliance for Europe*) research project. In fact, within the SERA project the capacity curves of equivalent-single-degree-of-freedom (ESDoF) systems representative of different classes of the European buildings portfolio were developed together with the corresponding fragility functions (Romao et al. 2019).

Although, for each building typology, the SERA project provided a set of capacity curves (Romao et al. 2019), the average capacity curves of each set are herein assumed to be representative of the entire typology. The state dependent fragilities are evaluated via the so-called *back-to-back incremental dynamic analysis* or IDA (Goda 2012; Ryu et al. 2011).

Proceedings of the 31st European Safety and Reliability Conference
Edited by Bruno Castanier, Marko Cepin, David Bigaud, and Christophe Berenguer
Published by Research Publishing, Singapore.
ISBN: 978-981-18-2016-8; doi:10.3850/978-981-18-2016-8_660-cd

The article is structured as follows: first, the characteristics of the set of analyzed structures representative of the Italian RC buildings are described. Then, the methodology is outlined along with the definition of damage states used for the fragility assessment. The chosen intensity measure and the identification of the number of ground motion records for the execution of the nonlinear-dynamic analysis are also discussed. Finally, the results are presented, discussing the lognormal assumption for the state-dependent fragilities.

2. RISE project structures

European existing structural typologies were identified in accordance with the building taxonomy developed within SERA (Romao et al. 2019) on the basis of an updated version of the international standard (i.e., the GEM building taxonomy; Brzev et al. 2013). This taxonomy catalogues buildings considering four main characteristics: primary construction material (e.g., reinforced concrete, unreinforced masonry, steel, etc.); typology of the lateral load resisting system (e.g., wall, moment frame, infilled frame, etc.); height expressed in terms of number of stories and seismic capacity-related properties (e.g., ductility and/or design later force), which depend on the evolution of seismic design in the country (e.g., Petruzzelli and Iervolino 2021); if available, information about the presence of structural irregularities is also provided.

2.1 Italian RC structures

The Italian RC existing structures analyzed in this study are represented by a set of eighteen infilled frame buildings, each representing a building class. The building classes are distinguished in terms of number of stories and level of seismic design. The buildings/classes considered have one to six stories and are also identified in terms of code level of seismic design, i.e., absent or low. Moreover, low-code structures are divided further, based on their design (lateral) base shear, which is either 5% or 10% of the building weight (i.e., the seismic coefficient).

3. Methodology

3.1 Capacity curves and damage states definition

The structures described in the previous section are analyzed using equivalent single-degree-of-freedom systems or ESDoF (e.g., Suzuki and Iervolino 2019) characterized by piece-wise linear backbone curves and a pinched hysteretic behavior exhibiting degradation of strength and of (unloading and reloading) stiffness under cyclic loading. An example of the cyclic response of the analyzed systems is shown in Fig. 1.

A generic backbone curve is presented in panel (a) of Fig. 2 in terms of displacements, δ, and ratio of the reacting force over the mass of the structure, F/m, along with the points identifying the capacity curve. Fig. 2a also shows the damage state thresholds considered in this study. Four damage states are considered ranging from *slight damage* (DS_1) to *collapse* (DS_4); all of them are defined according to the SERA project on the basis of Villar-Vega and Silva (2017) and Lagomarsino and Giovinazzi (2006).

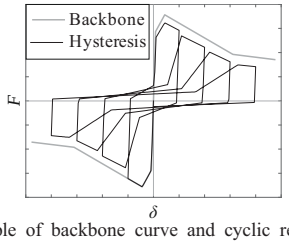

Fig. 1 Example of backbone curve and cyclic response of an inelastic SDoF system with pinched hysteretic behavior and cyclic strength and stiffness degradation.

The engineering demand parameter, EDP, adopted for the identification of the damage states is the (absolute value of the) maximum transient inelastic response in terms of displacement. Thus, in order to account for damage initiation in non-structural elements, DS_1 is considered to have been reached when the maximum displacement equals or exceeds 75% of the displacement corresponding to the value of F_c/m, δ_c, whereas the collapse corresponds to the ultimate displacement capacity of the structure, δ_u. The definition of the intermediate damage states, that is, moderate damage DS_2 and extensive damage DS_3, follows closely the proposal originally presented by Lagomarsino and Giovinazzi (2006). The thresholds of DS_2 and DS_3 are evenly spaced between the first and last damage state thresholds and are reached at the displacements equal to $0.50 \cdot \delta_c + 0.33 \cdot \delta_u$ and $0.25 \cdot \delta_c + 0.67 \cdot \delta_u$, respectively.

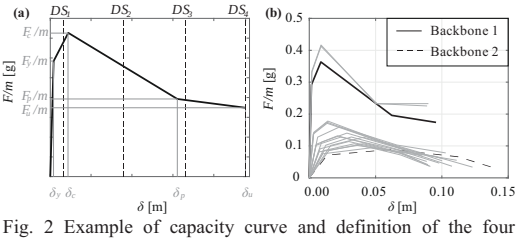

Fig. 2 Example of capacity curve and definition of the four damage states used in the study (a); capacity curves of the analyzed reinforced concrete structures (b).

The backbone curves of the eighteen structures considered here are shown in Fig. 2b (numerical values defining each curve are available at the data repository Romao et al. 2020). Each backbone in that figure, is determined as an average of the backbones of a multitude of structures comprising that class. More specifically, each piece-wise linear backbone is defined by four points $\left(\{\delta_y, F_y/m\}, \{\delta_c, F_c/m\}, \{\delta_p, F_p/m\}, \{\delta_u, F_u/m\}\right)$ – see Fig. 2a – and the displacement-acceleration coordinates of each point on the representative curve is evaluated as the geometric mean of the corresponding points defining the

capacity curves of the set. This geometric mean is obtained independently for the abscissa and the ordinate of each of the four points defining a representative average curve.

Two subsets of curves can be identified in the figure; they are representative of one-story and more-than-one-story (from two to six) buildings, respectively. More specifically, the curves with the highest values of F/m correspond to one-story structures among which one has absent level of seismic design whereas the other two have low code level with design lateral force equal to 5.0% and 10.0% of the building weight, respectively. The one-story buildings have vibration periods of about 0.15s whereas the structures with more than one story have periods ranging from 0.29s to 0.88s.

The state-dependent fragility curves were evaluated for the entire set of eighteen structures, whereas the choice of the intensity measure and the identification of the number of ground motion records for the execution of the nonlinear-dynamic analyses were conducted considering two benchmark systems among those reported in Fig. 2b. The backbone 1 (solid line) was selected to be representative of a one-story building, which has a vibration period; i.e., T_{el} equal to 0.15s. On the other hand, backbone 2 (dashed line) is considered representative of taller structures and corresponds to a six-story building with T_{el} equal to 0.88s.

3.2 Fragility assessment

In this study, fragility functions (i.e., for the undamaged structure) and state-dependent fragility functions are evaluated using IDA (Vamvatsikos and Cornell 2002) and back-to-back IDA, respectively. For a selected set of records, IDA collects the response of a non-linear undamaged structure to the records that are progressively scaled in amplitude to represent increasing levels of seismic intensity. The results of the procedure can be expressed using the IDA curves that represent the structural response via the selected EDP as a function of the intensity measure, IM .

Back-to-back IDA is an extension of IDA, in which the structural model is first subjected to a set of records shaking the structure at its intact state, causing it to reach a damage state DS_i. This is numerically simulated by having each record scaled in amplitude to the lowest IM value that causes the structure to reach the EDP threshold for damage state DS_i; thus, each record produces a different realization of the now-damaged structural model, which can be considered to have made the transition to DS_i. Subsequently, each damaged incarnation of the structural model (i.e., the ESDoF) is subjected to a second set of accelerograms. The records of the second set are scaled until the damaged structure reaches a more severe damage, say DS_j, where $j > i$.

Applying the *IM*-based approach to the results of IDA (Vamvatsikos and Cornell 2001) and back-to-back IDA, fragility functions and state-dependent fragility functions are evaluated. This approach consists in finding the realizations of the random variable $\left(IM_{DS}\right)$ that is the seismic intensity leading the structure to equal or exceed a certain damage state threshold. Assuming that this random variable follows a lognormal distribution, the fragility functions can be estimated according to Eq.(1):

$$P\left[DS_i \mid IM = im\right] = \\ = P\left[IM_{DS} \le im\right] = \Phi\left[\left(\ln(im) - \eta\right)/\beta\right], \quad (1)$$

where $P\left[DS_i \mid IM = im\right]$ is the sought conditional probability that, given the intensity measure value, $IM = im$, the undamaged structure reaches or exceeds a certain damage state DS_i, whereas η and β are the parameters (median and logarithmic standard deviation) of the assumed lognormal distribution, and $\Phi(\cdot)$ is the standard Gaussian (cumulative) function.

Concerning the state-dependent fragility, two probability distribution models are investigated; i.e., the lognormal and the gamma distributions. The former is already defined in Eq. (1) whereas the cumulative density function of the latter is provided by Eq. (2):

$$P\left[DS_j \mid DS_i \cap IM = im\right] = \frac{1}{b^a \cdot \Gamma(a)} \cdot \int_0^{im} z^{a-1} \cdot e^{\frac{z}{b}} \cdot \mathrm{d}z, \quad (2)$$

where $P\left[DS_j \mid DS_i \cap IM = im\right]$ is the probability that an already damaged structure transitions from a damage state DS_i to a more severe damage state DS_j, a and b are parameters, and $\Gamma(\cdot)$ is the Gamma function.[a]

In this study, the same set of records selected within the NESS dataset (Pacor et al., 2018) is used for both the IDA and the first and the second phase of back-to-back IDA. (The definition of the records set size is discussed in the following sections.) All the analyses (IDA and back-to-back IDA) are performed using the OpenSEES platform (Open System for Earthquake Engineering Simulation; McKenna, 2011) via a recent version of the DYANAS software (Baltzopoulos et al. 2018).

3.3 Choice of the intensity measure

In the assessment of structural response by means of dynamic analysis, the choice of the ground motion intensity measure is of primary importance. Traditionally, the IM is selected on the basis of its characteristics of sufficiency and efficiency which are strictly tied to the accuracy of the structural performance assessment (Luco 2002; Luco and Cornell 2007; Padgett et al. 2007). In fact, a *sufficient* IM renders the structural response conditionally independent, given the selected intensity measure, of the other earthquake characteristics involved in the seismic hazard assessment for the construction site (i.e., magnitude and source-to-site distance), whereas an

[a] The parameters of both gaussian and gamma models depend on the initial damage state and the exceeded damage threshold. However, such a dependency is not explicitly reported in Eq. (1) and Eq. (2) for the sake of simplicity.

efficient IM produces a relatively small variability in the structural response given the *IM*. The concepts of sufficiency and efficiency are used in this study to select the intensity measure for the execution of the IDA and back-to-back IDA.

The *IMs* known to allow an efficient prediction of the response of reinforced-concrete structures, in terms of maximum roof- or interstory-displacement, generally include elastic response spectral values and somehow account for spectral shape (Eads et al. 2015; Bojórquez and Iervolino 2011). In this study, four *IMs* were preliminarily considered as candidates: the elastic spectral acceleration at the period 0.3s; $Sa(T=0.3\,s)$ (in accordance with Romao et al. 2019), the elastic spectral acceleration at the vibration period of the undamaged system, $Sa(T_{el})$, the geometric mean of spectral accelerations Sa_{avg} (Baker and Cornell 2006) and the I_{NP} intensity measure (Bojórquez and Iervolino, 2011). Hereafter, the geometric mean of spectral accelerations $Sa_{avg}(T_1,T_2,\ldots,T_{20})$ is preliminarily evaluated considering twenty periods, equally spaced in a range between 0.05s and 3.0s, according to Eq. (3):

$$Sa_{avg}(T_1,T_2,\ldots,T_{20}) = \sqrt[20]{Sa(0.05\text{s})\cdot\ldots\cdot Sa(3.0\text{s})}\,. \quad (3)$$

The scalar intensity measure I_{NP} is also spectral-acceleration-based. In this case, it was defined using the same spectral ordinates considered for $Sa_{avg}(T_1,T_2,\ldots,T_{20})$, as shown in Eq. (4):

$$I_{NP}(T_1,T_2,\ldots,T_{20}) = Sa(T_{el})\cdot\left[\frac{Sa_{avg}(T_1,T_2,\ldots,T_{20})}{Sa(T_{el})}\right]^{\alpha}, \quad (4)$$

where α is a parameter that, strictly speaking, requires structure-specific calibration, but is assumed equal to 0.4 in the following (Bojórquez and Iervolino, 2011). (It can be noted that $Sa_{avg}(T_1,T_2,\ldots,T_{20})$ can be regarded as a special case of $I_{NP}(T_1,T_2,\ldots,T_{20})$, for $\alpha=1$.)

Among the cited *IMs*, one had to be selected for computing fragility functions and state-dependent fragility function of all the analyzed buildings. To this aim, the two already mentioned benchmark systems are considered (see Fig. 2b).

As pertaining to sufficiency, past research has shown that intensity measures that account for spectral shape in a range of periods (i.e., Sa_{avg} and I_{NP} among those considered here) seem to perform better than single-spectral-ordinate *IMs* at higher damage states. This can be intuitively attributed to the fact that a damaged structure's stiffness is lower than what it was in intact conditions and, consequently, the range of vibration periods overall influencing the dynamic response increases.

On the other hand, to have an indication of the efficiency of the four investigated intensity measures, the coefficient of variation of the IM_{DS}, $COV_{IM_{DS}}$, is evaluated for increasing values of failure threshold, $\delta_{\max}$. Fig. 3 shows the values of $COV_{IM_{DS}}$ assessed for the four different *IMs* and the two benchmark systems.

The figure shows that Sa_{avg} and I_{NP} are more efficient intensity measures than the single spectral ordinates, as expected and confirms the findings of past research, that *IM* efficiency is damage-state-dependent (Kazantzi and Vamvatsikos 2015). For example, a previous work has indicated that the efficiency of I_{NP} with different α values (0.3 or 1) varies with damage state (Baltzopoulos, Iervolino, et al. 2019). For these preliminary analyses, Sa_{avg} was used as the *IM* of choice, in other words I_{NP} with $\alpha=1$.

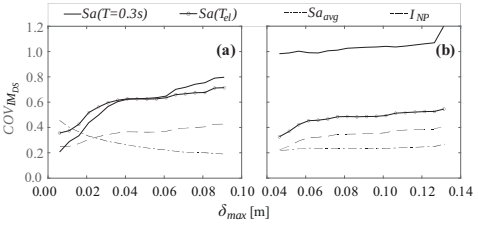

Fig. 3 $COV_{IM_{DS}}$ as a function of $\delta_{\max}$ evaluated for the four *IMs*, for the first (a) and the second system (b).

3.4 Number of records

The issue addressed in this section concerns the identification of the number of ground motions used to perform dynamic analyses in other to balance the computational costs and the accuracy in fragility assessment. To this end, the statistical concept of estimation uncertainty (Iervolino, 2017; Baltzopoulos et al. 2019) is applied to the estimates of the parameters defining the parametric fragility Eq. (1).

The record sample size is selected trying to limit the estimation error of the two parameters η and β that define the fragility functions of the intact structures under the lognormal assumption. Although the gamma distribution is also contemplated as an alternative to the lognormal for the state-dependent fragilities, this consideration of estimation uncertainty is limited to the intact structures' fragility and the lognormal model. The quantitative measure of the uncertainty in the fragility assessment used in this study, is the coefficients of variation $COV_{\hat{\eta},}$ and $COV_{\hat{\beta}}$ evaluated for the estimators of the median $\hat{\eta}$ and of the standard deviation $\hat{\beta}$, respectively. The coefficient of variation $COV_{\hat{\vartheta},}$ of a generic estimator $\hat{\vartheta}$ is defined as the square root of $VAR[\hat{\vartheta}]$ divided by $E[\hat{\vartheta}]$, that is the ratio of the standard deviation and the expected value of $\hat{\vartheta}$. The terms

$VAR\left[\hat{\vartheta}\right]$ and $E\left[\hat{\vartheta}\right]$ can be substituted by their estimates obtained using a parametric resampling scheme proposed in Baltzopoulos et al. (2019). This procedure entails randomly sampling l times (in this case 5000 times) from an assumed reference fragility model; i.e., the distribution of IM_{DS} defined by the results of IDA performed using the entire fifty-record set. This is repeated for a number of times, each time extracting different samples sizes N, varying from 20 to 50. In this context, sample size ostensibly corresponds to the number of records used in dynamic analysis, and $COV_{\hat{\vartheta}}$ is approximated as:

$$COV_{\hat{\vartheta}} = \frac{\sqrt{VAR\left[\hat{\vartheta}\right]}}{E\left[\hat{\vartheta}\right]} \approx \frac{\sqrt{\frac{1}{l-1}\cdot\sum_{j=1}^{l}\left(\hat{\vartheta}_j - \frac{1}{l}\cdot\sum_{k=1}^{l}\hat{\vartheta}_k\right)^2}}{\frac{1}{l}\cdot\sum_{j=1}^{l}\hat{\vartheta}_j}. \quad (5)$$

This procedure is implemented for the two benchmark systems showed in Fig. 2b for the fragilities to collapse (i.e., DS_4). In Fig. 4, the results obtained varying the size of the records set N from 20 to 50 are reported. Through the described procedure, it is decided to use a number of records equal to 35 that allows to maintain $COV_{\hat{\beta}}$ between 10% and 15% for the two systems and $COV_{\hat{\eta}}$ below 10%. Moreover, Fig. 4 also shows $COV_{\hat{\eta}}$ and $COV_{\hat{\beta}}$, evaluated for all the other RC structures using 35 records in order to verify that the associated coefficients of variation of the two estimators also adhere to these limitations.

The defined set of 35 records is used for the execution of both IDA and back-to-back IDA.

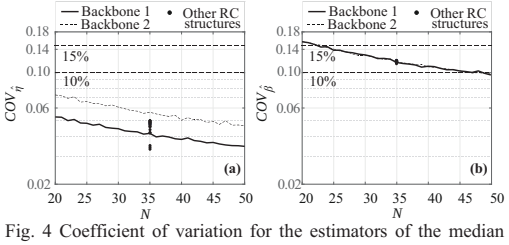

Fig. 4 Coefficient of variation for the estimators of the median $COV_{\hat{\eta}}$ (a) and the standard deviation $COV_{\hat{\beta}}$ (b) of the DS_4 fragility curve of RC structures against the number of records N.

4. Results

4.1 Classical curves

Fig. 5 shows the fragility curves obtained analyzing the set of eighteen RC structures via IDA. Each panel of Fig. 5 shows the fragility curves of the intact structures evaluated for each arriving damage state according to Eq. (1); i.e. panel (a) refers to DS_1; panel (b) to DS_2; panel (c) to DS_3 and panel (d) to DS_4.

The values of median, η, and logarithmic standard deviation, β, defining the parametric fragilities of intact structures numbered from 1 to 18 are reported in Table 1. The table also shows for each structure the adopted code level of seismic design (absent or low); the height expressed in terms of number of stories (H) and the design lateral force (0%, 5% or 10% of the building weight). As previously mentioned, the one-story buildings are always less fragile than the other RC structures for all damage states considered.

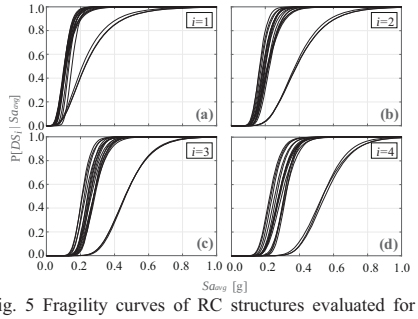

Fig. 5 Fragility curves of RC structures evaluated for the four damage states DS_1 (a); DS_2 (b); DS_3 (c) and DS_4 (d).

4.2 State-dependent curves

For the state-dependent fragilities, the assumption of a lognormal distribution or, alternatively, of a gamma distribution is investigated. Fig. 6 shows the comparison between the non-parametric state-dependent fragilities (identified by the *non-par* subscript in the legend) and the parametric ones evaluated using the lognormal and the gamma distribution (*log* and *gamma* subscripts), panel (a) and panel (b) respectively. The state-dependent fragility curves reported in Fig. 6 refer to the same starting state DS_2 but have different final states, DS_3 or DS_4.

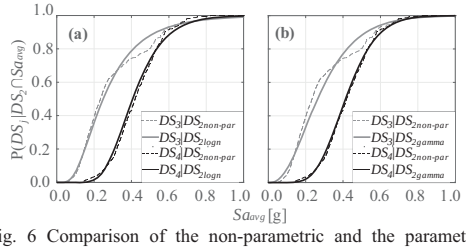

Fig. 6 Comparison of the non-parametric and the parametric state-dependent fragility curves evaluated for the benchmark system 1 assuming the lognormal distribution (a) or the gamma distribution (b).

It was observed that, among analyzed cases, the lognormal distribution may be more suitable for modelling fragility for some of the damage state transitions (generally from DS_2 to DS_3 and from DS_3 to DS_4) whereas the gamma distribution appears more suitable for the other transitions, as shown in Fig. 6 for one case of the benchmark system 1. It can be seen that neither distribution can adequately capture the non-parametric results at large intensity levels,

due to the limitation of being defined by only two parameters; however the left tail is generally more relevant for risk assessment. In this study the gamma distribution was chosen to represent the state-dependent fragilities. Table 2 collects the values of the parameters a and b defining the gamma distribution, Eq. (2); i.e., the parametric state-dependent fragility curves for the eighteen RC structures. In the table, the fifth column given the initial damage state wheres the damage state reported in the rest of the row represent the arrival damage states.

Table 1. Median η and logarithmic standard deviation β defining the fragility curves of RC intact structures (*IM* in g).[b]

#	Code Level	H	Lateral Force Coefficient (%)	MEDIAN η				SIGMA β			
				DS_1	DS_2	DS_3	DS_4	DS_1	DS_2	DS_3	DS_4
1	Absent	1	0.00	0.21	0.37	0.46	0.53	0.54	0.34	0.25	0.22
2	Absent	2	0.00	0.11	0.21	0.28	0.31	0.44	0.29	0.21	0.17
3	Absent	3	0.00	0.11	0.20	0.26	0.28	0.36	0.20	0.18	0.21
4	Absent	4	0.00	0.13	0.20	0.25	0.27	0.28	0.20	0.22	0.23
5	Absent	5	0.00	0.13	0.21	0.26	0.28	0.24	0.23	0.23	0.23
6	Absent	6	0.00	0.15	0.22	0.28	0.29	0.23	0.23	0.24	0.23
7	Low	1	5.00	0.23	0.38	0.46	0.54	0.49	0.32	0.24	0.20
8	Low	2	5.00	0.11	0.21	0.28	0.31	0.39	0.26	0.18	0.14
9	Low	3	5.00	0.10	0.19	0.24	0.26	0.38	0.24	0.18	0.20
10	Low	4	5.00	0.11	0.18	0.22	0.24	0.34	0.24	0.20	0.22
11	Low	5	5.00	0.10	0.17	0.21	0.23	0.30	0.21	0.20	0.24
12	Low	6	5.00	0.11	0.17	0.21	0.22	0.31	0.25	0.22	0.24
13	Low	1	10.00	0.23	0.38	0.46	0.55	0.44	0.30	0.22	0.18
14	Low	2	10.00	0.11	0.22	0.28	0.32	0.43	0.28	0.19	0.14
15	Low	3	10.00	0.12	0.22	0.28	0.31	0.39	0.25	0.18	0.20
16	Low	4	10.00	0.11	0.20	0.25	0.28	0.38	0.25	0.19	0.22
17	Low	5	10.00	0.10	0.19	0.24	0.28	0.33	0.23	0.21	0.23
18	Low	6	10.00	0.11	0.18	0.23	0.25	0.31	0.25	0.23	0.22

Table 2. Parameters a and b defining the state-dependent fragility curves of RC structures (*IM* in g).[c]

#	Code Level	H	Lateral Force Coefficient (%)	DS	DS_2		DS_3		DS_4	
					a	b	a	b	a	b
1	Absent	1	0.00	DS_1	8.862	0.041	14.856	0.031	21.319	0.025
				DS_2	\	\	3.503	0.084	10.272	0.042
				DS_3	\	\	\	\	3.433	0.077
2	Absent	2	0.00	DS_1	11.260	0.017	22.863	0.012	31.623	0.010
				DS_2	\	\	3.436	0.041	10.238	0.022
				DS_3	\	\	\	\	3.488	0.038
3	Absent	3	0.00	DS_1	10.360	0.014	21.059	0.011	23.094	0.012
				DS_2	\	\	4.092	0.028	8.962	0.021
				DS_3	\	\	\	\	2.779	0.047
4	Absent	4	0.00	DS_1	6.431	0.018	18.191	0.011	20.900	0.012
				DS_2	\	\	3.674	0.029	6.563	0.025
				DS_3	\	\	\	\	2.428	0.046
5	Absent	5	0.00	DS_1	5.400	0.022	14.258	0.015	18.754	0.014
				DS_2	\	\	4.426	0.022	6.482	0.025
				DS_3	\	\	\	\	2.967	0.039

[b] In some cases, the results are corrected reducing the standard deviation up to a maximum of 20% in order to avoid the intersection between the lognormal fragility curves referring to different damage states (such intersections are not observed on non-parametric results).

[c] In some cases, the results are corrected reducing the standard deviation up to a maximum of 7% in order to avoid the intersection between state-dependent gamma fragility curves starting from the same damage state and having different final damage state (such intersections are not observed on non-parametric results).

Table 2. (*Continued*) Parameters a and b defining the state-dependent fragility curves of RC structures (*IM* in g).

#	Code Level	H	Lateral Force Coefficient (%)	DS	DS_2		DS_3		DS_4	
					a	b	a	b	a	b
				DS_1	5.628	0.021	12.306	0.017	18.326	0.014
6	Absent	6	0.00	DS_2	\	\	3.779	0.029	5.665	0.030
				DS_3	\	\	\	\	2.634	0.040
				DS_1	7.757	0.048	13.342	0.034	16.234	0.033
7	Low	1	5.00	DS_2	\	\	3.213	0.091	8.512	0.048
				DS_3	\	\	\	\	3.106	0.084
				DS_1	10.989	0.017	22.268	0.012	32.447	0.009
8	Low	2	5.00	DS_2	\	\	3.468	0.039	10.716	0.021
				DS_3	\	\	\	\	2.941	0.055
				DS_1	10.845	0.014	22.741	0.010	22.460	0.011
9	Low	3	5.00	DS_2	\	\	3.770	0.031	9.739	0.019
				DS_3	\	\	\	\	3.024	0.035
				DS_1	8.447	0.014	17.706	0.011	20.021	0.012
10	Low	4	5.00	DS_2	\	\	4.085	0.024	7.943	0.020
				DS_3	\	\	\	\	3.164	0.029
				DS_1	8.322	0.015	16.546	0.011	17.896	0.012
11	Low	5	5.00	DS_2	\	\	4.949	0.018	8.093	0.018
				DS_3	\	\	\	\	2.896	0.031
				DS_1	6.632	0.019	13.263	0.014	17.847	0.012
12	Low DS_1	6	5.00	DS_2	\	\	4.913	0.018	7.425	0.019
				DS_3	\	\	\	\	3.131	0.025
				DS_1	7.460	0.051	13.194	0.035	16.391	0.033
13	Low	1	10.00	DS_2	\	\	2.923	0.088	8.768	0.045
				DS_3	\	\	\	\	3.037	0.083
					11.036	0.017	23.051	0.012	31.845	0.010
14	Low	2	10.00	DS_2	\	\	3.297	0.047	10.544	0.023
				DS_3	\	\	\	\	2.957	0.048
				DS_1	11.013	0.016	23.785	0.011	22.890	0.013
15	Low	3	10.00	DS_2	\	\	6.339	0.017	11.358	0.018
				DS_3	\	\	\	\	3.946	0.029
				DS_1	10.556	0.015	18.526	0.012	20.144	0.013
16	Low	4	10.00	DS_2	\	\	5.305	0.021	10.303	0.018
				DS_3	\	\	\	\	3.148	0.036
				DS_1	12.261	0.014	17.966	0.013	19.069	0.015
17	Low	5	10.00	DS_2	\	\	5.786	0.018	9.900	0.019
				DS_3	\	\	\	\	3.367	0.031
				DS_1	8.885	0.017	15.674	0.014	18.377	0.013
18	Low	6	10.00	DS_2	\	\	4.463	0.023	7.226	0.023
				DS_3	\	\	\	\	2.940	0.033

5. Conclusions

This study shows the preliminary results towards the assessment of state-dependent fragility functions for Italian reinforced concrete structures taken from the outcomes of the SERA project. Fragility assessment was conducted via back-to-back IDA of an ESDoF approximation of single structures, each representing a building class. In this context, two issues significantly affecting the assessment

were addressed: the choice of the intensity measure and the identification of the number of ground motion records for the execution of nonlinear dynamic analyses. Based on comparison of different intensity measures, it was confirmed that those entailing a geometric mean of spectral accelerations, that is, Sa_{avg} and I_{NP}, were to be preferred due to exhibiting greater efficiency than single-period spectral ordinates. In lack of a specific calibration of the I_{NP} intensity measure at this stage, Sa_{avg} was selected for the state-dependent fragilities. As far as the number of records is concerned, a set of 35 ground motions was used as a compromise between computational costs and the precision in fragility assessment, based on the statistical inference concept of estimation uncertainty.

The fragility curves for the intact structures were modelled assuming a lognormal distribution; on the other hand, for the state-dependent fragility functions, the model chosen to describe the non-parametric fragilities was the gamma distribution.

Acknowledgement

The work presented in this paper was developed within the H2020-SC5-2019 Real-time Earthquake Risk Reduction for a Resilient Europe (RISE) project, Grant Agreement 821115. The ECH2020 SERA (Seismology and Earthquake Engineering Research Infrastructure Alliance for Europe) project is gratefully acknowledged for sharing data needed to perform the analyses discussed in the paper.

References

Baker, J. W., and Cornell, C. A. (2006). Spectral shape, epsilon and record selection. *Earthquake Engineering and Structural Dynamics 35* , 1077–1095.

Baltzopoulos, G., Baraschino, R., and Iervolino, I. (2018). On the number of records for structural risk estimation in PBEE. *Earthquake Engineering & Structural Dynamics*.

Baltzopoulos, G., Baraschino, R., Iervolino, I., and Vamvatsikos, D. (2018). Dynamic analysis of single-degree-of-freedom systems (DYANAS): a graphical user interface for OpenSEES. *Engineering Structures 177* , 395–408.

Baltzopoulos, G., Iervolino, I., and Baraschino, R. (2019). Ground motion sample size vs estimation uncertainty in seismic risk. *13th International Conference on Applications of Statistics and Probability in Civil Engineering, ICASP 2019*.

Bojórquez, E., and Iervolino, I. (2011). Spectral shape proxies and nonlinear structural response. *Soil Dynamics and Earthquake Engineering 31* , 996–1008.

Brzev, S., Scawthorn, C., Charleson, A. W., Allen, L., Greene, M., Jaiswal, K., and Silva, V. (2013). GEM Building Taxonomy Version 2.0. *GEM Technical Report 02* , 188.

Eads, L., Miranda, E., and Lignos, D. G. (2015). Average spectral acceleration as an intensity measure for collapse risk assessment. *Earthquake Engineering and Structural Dynamics 44* , 2057–2073.

Goda, K. (2012). Nonlinear response potential of Mainshock-Aftershock sequences from Japanese earthquakes. *Bulletin of the Seismological Society of America 102* , 2139–2156.

Iervolino, I. (2017). Assessing uncertainty in estimation of seismic response for PBEE. *Earthquake Engineering & Structural Dynamics 46* , 1711–1723.

Iervolino, I., Chioccarelli, E., and Suzuki, A. (2020). Seismic damage accumulation in multiple mainshock–aftershock sequences. *Earthquake Engineering and Structural Dynamics 49* , 1007–1027.

Iervolino, I., Giorgio, M., and Chioccarelli, E. (2016). Markovian modeling of seismic damage accumulation. *Earthquake Engineering & Structural Dynamics 45* , 441–461.

Iervolino, I., Manfredi, G., Polese, M., Verderame, G. M., and Fabbrocino, G. (2007). Seismic risk of R.C. building classes. *Engineering Structures 29* , 813–820.

Kazantzi, A. K., and Vamvatsikos, D. (2015). Intensity measure selection for vulnerability studies of building classes. *Earthquake Engineering and Structural Dynamics 44* , 2677–2694.

Lagomarsino, S., and Giovinazzi, S. (2006). Macroseismic and mechanical models for the vulnerability and damage assessment of current buildings. *Bulletin of Earthquake Engineering 4* , 415–443.

Luco, N. (2002). Probabilistic seismic demand analysis, SMRF connection fractures, and near-source effects. In *Department of Civil and Environmental Engineering of Stanford University*.

Luco, N., and Cornell, C. A. (2007). Structure-specific scalar intensity measures for near-source and ordinary earthquake ground motions. *Earthquake Spectra 23* , 357–392.

McKenna, F. (2011). OpenSEES: A framework for earthquake engineering simulation. *Computing in Science and Engineering 13* , 58–66.

Pacor, F., Felicetta, C., Lanzano, G., Sgobba, S., Puglia, R., D'Amico, M., Russo, E., Baltzopoulos, G., and Iervolino, I. (2018). NESS v1.0: A worldwide collection of strong-motion data to investigate near source effects. *Seismological Research Letters*.

Padgett, J. E., Nielson, B. G., and Desroches, R. (2007). Selection of optimal intensity measures in probabilistic seismic demand models of highway bridge portfolios. *Earthquake Engineering & Structural Dynamics 37* , 711–725.

Petruzzelli, F., and Iervolino, I. (2021). NODE: a large-scale seismic risk prioritization tool for Italy based on nominal structural performance. *Bulletin of Earthquake Engineering 19* , 2763–2796.

Romao, X., Castro, J. M., Pereira, N., Crowley, H., Silva, V., Martins, L., and Rodrigues, D. (2019). *Project SERA. Deliverable 26.5: European physical vulnerability models.*

Romao, X., Pereira, N., Castro, J. M., De Maio, F., Crowley, H., and Silva, V. (2020). *European Building Vulnerability Data Repository (Version v1.2) [Data set]. Zenodo.*

Ryu, H., Luco, N., Uma, S. R., and Liel, A. B. (2011). Developing fragilities for mainshock-damaged structures through incremental dynamic analysis. *Proceedings of the Ninth Pacific Conference on Earthquake Engineering 225* , 8.

Suzuki, A., and Iervolino, I. (2019). Seismic Fragility of Code-conforming Italian Buildings Based on SDoF Approximation. *Journal of Earthquake Engineering*.

Vamvatsikos, D., and Cornell, C. A. (2001). Incremental Dynamic Analysis. *Earthquake Engineering and Structural Dynamics 31* , 491–514.

Vamvatsikos, D., and Cornell, C. A. (2002). Incremental dynamic analysis. *Earthquake Engineering and Structural Dynamics 31* , 491–514.

Villar-Vega, M., and Silva, V. (2017). Assessment of earthquake damage considering the characteristics of past events in South America. *Soil Dynamics and Earthquake Engineering 99* , 86–96.